DUV Autofluorescence Microscopy for Cell Biology and Tissue Histology Biology of the Cell Biology of the Cell

Frederic Jamme, Slávka Kaščáková, Sandrine Villette, Fatma Allouche, Stéphane Pallu, Valerie Rouam, Matthieu M. Refregiers

Biology of the Cell

DUV Autofluorescence Microscopy for Cell Biology and Tissue Histology

Journal:	*Biology of the Cell*
Manuscript ID:	Draft
Wiley - Manuscript type:	Research Article
Date Submitted by the Author:	n/a
Complete List of Authors:	Jamme, Frédéric; Synchrotron SOLEIL, DISCO Beamline; INRA, UAR 1008 CEPIA Kascakova, Slavka; Synchrotron SOLEIL, DISCO Beamline Villette, Sandrine; CNRS, CBM UPR4301 Allouche, Fatma; INRA, UAR 1008 CEPIA Pallu, Stéphane; Université d'Orléans, Rouam, Valérie; Synchrotron SOLEIL, DISCO Beamline Refregiers, Matthieu; Synchrotron SOLEIL, DISCO Beamline
Keywords:	Cellular imaging, Plants, Oncology/cancer, Metabolism

DUV Autofluorescence Microscopy for Cell Biology and Tissue Histology

Frédéric Jamme[1, 2, *], Slavka Kascakova[1], Sandrine Villette[3], Fatma Allouche[2], Stéphane Pallu[4], Valérie Rouam[1], Matthieu Réfrégiers[1]

1- Synchrotron SOLEIL, L'Orme des Merisiers, Gif sur Yvette, France.

2- INRA, UAR 1008 CEPIA, Rue de la Géraudière, F-44316 Nantes, France.

3- Centre de Biophysique Moléculaire, CNRS UPR4301, Rue Charles Sadron, 45071 Orléans cedex 2, France.

4- INSERM U-658, Hôpital Porte Madeleine, BP 2439, 45032 Orléans cedex 01, France.

Corresponding author : Frédéric Jamme

phone : +33-(0)1-69 35 9686

fax : +33-(0)1-69 35 9456

E-mail : jamme@synchrotron-soleil.fr

Keywords: Autofluorescence, UV, DUV, synchrotron, microspectroscopy

Abbreviations: VUV, vacuum ultraviolet; DUV, deep ultraviolet; HeLa, Human cervix epithelial cell line; FAD, Flavin adenine dinucleotide; FPs, Fluorescent proteins; BPA, Bisphenol A; PVC, Polyvinyl chloride.

Acknowledgement

Part of this work was supported by the Région Centre (FRANCE). Synchrotron SOLEIL support through projects #20100064, 201000181, 20100949 and 20110131 is acknowledged.

Graphical Abstract

Ultraviolet induced autofluorescence of cells is often, if not ever, considered as a parasitic signal that must be minimized. Using a tuneable ultraviolet source, it is possible to exploit the autofluorescence signal for obtaining valuable information on selected cells either isolated or in tissular context.

Abstract

Autofluorescence is a powerful tool for molecular histology and follow up of metabolic processes in mammal and vegetal samples. However, at the microscopic scale, it is limited to visible and near infrared excitation of the samples.

Because several interesting naturally occurring fluorochromes absorb in the UV and DUV, we have developed a synchrotron-coupled DUV microspectrofluorimeter. Available since 2010, this new DUV microscope gives promising results for the study of representative samples, cultured cells, bone sections and maize stems.

An extended selection of natural occurring autofluorescent probes is presented with all their spectral characteristics; their distribution in various biological samples is also shown. We demonstrate that DUV autofluorescence is a powerful tool for tissue histology and cell biology.

Introduction

The ultraviolet autofluorescence of cells and tissues has long been evaluated for its diagnosis potential. However, since sources and microscopes that allow obtaining reliable information in the DUV (bellow 350 nm) are difficult to obtain and couple for medical diagnosis imaging of tissues, most of the medical diagnosis concentrated on the autofluorescence spectroscopy and microscopy of endogenous probes such as porphyrins which have emission in the visible range.

Synchrotron radiation is a broadband light that can be monochromatized in almost any energy range. The DISCO beamline at the synchrotron SOLEIL optimizes the vacuum ultraviolet (VUV) to the visible range of the spectrum (Giuliani et al., 2009). The deep ultraviolet (DUV) energies accessible on two microscopes at atmospheric pressure are defined by quartz cut-off, starting from 200 nm to longer wavelengths (600 nm) (Jamme et al., 2010; Tawil et al., 2011). For biological relevance, we specifically focus on the range between 200 and 350 nm that is very rarely covered especially under 250 nm.

The deep ultraviolet range is of particular interest for studying biomacromolecules due to their absorption in this energy range. While spectrometers can often go down to this range to study isolated biomacromolecules, microscopes are usually very limited in this range with either 350 nm cut-off or access to only a limited number of excitation wavelengths.

Köhler developed deep ultraviolet microscopy in 1904 as a bright field transmission technique (Kohler, 1904). This was implemented for one main reason: to improve the spatial resolution of cellular imaging. It passed through the century allowing seeing the unseen, namely nucleic acids in cells (Mellors et al., 1950), and to observe colour

differences in tumours under UV excitation for cancer diagnosis (Ludford et al., 1948). Thanks to developments in detectors, it became a quantitative method to observe protein and DNA contrast at 280 and 260 nm (Zeskind et al., 2007). However, due to differences of optical density in deep UV transmission images, scattering errors are difficult to avoid and interpreting DUV images are more challenging than spectral imaging using our confocal DUV fluorescence microscope.

Nonlinear microscopy is an alternative approach for live tissue visualization of autofluorescent compounds (Zipfel et al., 2003; Diaspro et al., 2005). The infrared photons exciting the sample are an asset, allowing deep tissue penetration in the optical window of living tissue. However this methodology present two inconvenient as compared to DUV monophotonic excitation; being a non-linear process relying onto infrared photons, its resolution remains in the µm range, second, the two photon action spectrum are very broad and do not permit as fine selectivity as DUV microscopy.

While most biomolecules do present a contrast in DUV transmission microscopy, few of them will reemit fluorescence. This autofluorescence is very important in a sense that it permits better discrimination of molecules. Moreover, following autofluorescence opens label free studies of molecules of interest without any external probes or radiolabelling that could impair activity of the molecule of interest (Tawil et al., 2011; Batard et al., 2011).

While many studies were conducted in DUV fluorescence spectroscopy as a diagnosis tool, mainly for cancer [(Wagnieres et al., 1998; Pavlova et al., 2008), very few were conducted on DUV fluorescence microscopy or microspectrofluorimetry on biopsies and tissues. Most of them were using excitation wavelength longer than 350

nm, mostly due to the lack of laser lines below this value, despite very promising sensibility and sensitivity using DUV excitation (Ramanujam et al., 1994). Indeed, many endogenous fluorophores have an absorption / excitability maximum in DUV below 350 nm, especially tryptophan (Wagnieres et al., 1998). Signal attributed to tryptophan typically exhibits fluorescence intensities orders of magnitude greater than those from other endogenous fluorophores. And although its fluorescence can serve as an additional marker for monitoring cellular status (Ramanujam, 2000) due to lack of DUV fluorescence microscopy, this fluorophore is often ignored.

In addition, considering the recent work by Cox et al, no specific labels are needed for super resolution microscopy techniques (Cox et al., 2011). Therefore, aufluorescent (free labeling) molecules blinking and bleaching could be use to improve resolution.

In this study, we first present the main autofluorescent biomolecules spectra detected in cells or tissues. Then, we demonstrate the usefulness of DUV microscopy for in situ studies of cell biology and tissue histology. We choose the most occurring natural fluorochromes and representative samples of cells either isolated or in various tissular surrounding, namely cultured cancerous cells, osteocytes in a bone context, vegetal cells as appropriate illustrative examples.

Results

Isolated auto fluorescent compounds

When measuring endogenous signals, no additional dyes or contrast agents are necessary to determine native characteristics of cells or tissues. However, when considering an autofluorescence signal from biologic material, all the contributing fluorophores and chromophores must be accounted for (due to excitation, emission and absorption spectra overlapping). To identify the major biological autofluorescence compounds in DUV, we selected and recorded their fluorescence emission and excitation spectra (Figures 1-4). Most of them have a maximum excitation peak below 350 nm. One can notice that each of them have distinct spectrum (maximum peak). However, several chromophores, such as pyridoxine, collagen and elastin, do present very close emission spectra that become difficult to discriminate without spectral detection. In those cases, fine-tuning of the excitation (Figure 1) may permit better separation of the species by altering their relative intensities.

The fluorophores were measured in PBS at pH = 7 (Figure 1), which does not represent a realistic in vitro and/or in vivo situation. Indeed, the spectroscopic characteristics of fluorophores can change due to environment-related effects and spectral shifts may occur. A bathochromic shift of absorption maxima of bilirubin is observed when bound to HSA, compared to free (and unbound) bilirubin in PBS (Kanick et al., 2010). Also coenzymes such as NAD(P)H reveals distinct spectroscopic characteristics, as shown on Figure 2. Free NADH in PBS has an emission maximum located at 460 nm, while, a hypsochromic shift of 10 nm in the position of its fluorescence maximum is observed when it is bound to alcohol

dehydrogenase. The knowledge of those spectral differences of NAD(P)H allowed previously to envisage the monitoring and quantification of total NAD(P)H concentration (free and bound NAD(P)H), which is an important parameter for the interpretation of cellular metabolism (Paul and Schneckenburger, 1996; Villette et al., 2006). However, the example of bilirubin or NAD(P)H shows also the difficulty of the identification of spectral components within the global autofluorescence signal of cell or tissue. It becomes obvious that the detailed knowledge of the influence of factors such as pH, binding, hydrophilicity/lipophilicity on the spectral properties of fluorophores is necessary to identify the chemical composition of biological material under investigation.

Grass lignocelluloses are a major resource in the emerging cellulose to ethanol strategy for biofuels (Anderson and Akin, 2008). However, the potential bioconversion of carbohydrates is limited by the associated aromatic constituents within the grass fibre. These aromatics include both lignin and low-molecular weight phenolic acids. The two main ester linked phenolics (ferulic and para-coumaric acids) can be differentiated by DUV absorption maximums near 326 nm and 314 nm, respectively. As shown in Figure 4, ferulic acid and para-coumaric acid have an emission peak centred at 415 and 400 nm, respectively while lignin shows a maximum of autofluorescence around 475 nm. Ferulic acid and para-coumaric acid can hardly be distinguished from each other using conventional fluorescence microscope, infrared or Raman spectroscopies (Saadi et al., 1998; Robert et al., 2010).

Synchrotron flux profile and microscope spectral response

The flux was measured (Ph/s) at the entrance of the microscope using a calibrated photodiode (AXUV 100, IRD, CA, USA) coupled to a current amplifier (DLPCA-200, laser Components, UK). As described previously (Jamme et al., 2010), the excitation light is provided by a bending magnet emission on the DISCO beamline at synchrotron SOLEIL (Giuliani et al., 2009). White beam from 180 to 600 nm is monochromatized by an iHR320 (Jobin-Yvon, FR) equipped with a 100 grooves per millimetre grating with a 240 nm peak efficiency (Spectrum Scientific, Inc, Irvine, CA, USA). Thus the flux variation observed, shown in Figure 5, is mainly attributed to the excitation monochromator grating response convoluted by the transmission view port (UV fused silica, MPF, SC, USA).

The spectral response of the microscope was measured using a calibrated lamp (QTH 45W, Microcontrole, FR) through the 40X objective (Ultrafluar, Zeiss, D) and calculating the ratio between the detected signal and the known emittance of the lamp (Figure 5). The response variation observed in Figure 5 is mostly attributed to the emission spectrometer gratings (T64000, Horiba Jobin-Yvon, FR).

Applications to cell and tissues

Isolated living cells

In order to assess the distribution of endogenous fluorophore in single cell, the whole living cell was scanned under 275 nm excitation with 1s exposure time and the fluorescence emission spectra of the cell were recorded at each pixel. The Figure 6 represents the spectra of autofluorescence obtained from the highlighted pixels. As it can be seen from Figure 6, in a simplified model, the emission spectrum of a living cell is mainly tryptophan and tyrosine fluorescence arising from the proteins. In a

cellular context, due to environmental influence, tryptophan fluoresces at 335 nm and tyrosine at 306 nm (Villette et al., 2006; Lakowicz, 2006).

Maize stem cell walls

Improving the ease and yield of cell wall saccharification represents the major technological hurdle that must be overcome before the full vision of the plant-fuelled biorefinery can be realized. Thus, mapping of the spatial distribution of the fluorescent species at a micrometric resolution as a function of growth stage allows the assessment of the best enzymatic treatments and high yield of recovery of useful chemical for biofuel or biomaterials productions can be foreseen.

As shown in Figure 7, the spectral images studied recorded using a 275 nm excitation, covered a region in the vascular bundle of the maize internodes cross-section that contained mainly three cell types: parenchyma, sclerenchyma and phloem cells. For clarity, average spectra were calculated for each cell type region as shown in Figure 7 (bottom left). In the case of the phloem, a peak around 415 nm was observed in the spectra while, in the case of sclerenchyma, the peak was centred on 420 nm and fluorescence was also detected from 440 nm to 540 nm. This confirmed that sclerenchyma cell walls contained lignin while phloem cell walls did not (Allouche et al., 2012). In addition, multivariate data analysis reveals that para-coumaric acid was found negatively correlated to lignin (Allouche et al., 2012).

Biopsies

The main features observable on tissues under 280 nm excitation are related to tryptophan, tyrosine and in a lesser extent to constitutive proteins (Petit et al., 2010).

However, when shifting the excitation wavelength to 340 nm, the collagen fluorescence increases significantly.

Bones

Osteoporotic fractures represent a significant public health concern. Bone quality (bone microarchitecture, collagen content) was investigated at subcellular resolution. Synchrotron DUV spectroscopy allows to characterize and distinguish biochemical content of the osteocytes and their surrounding matrix, since osteocytes are considered as the orchestrator of the bone remodelling (Rochefort et al., 2010). In a rat experimental model of alcoholic induced osteoporosis, sections of cortical bone were investigated and osteocytes autofluorescence images are presented in Figure 8. The fluorescence emission spectra present three peaks situated at 305 nm, 333 nm and 385 nm, attributed to tyrosine, tryptophan and collagen respectively. The ratio between tyrosine and tryptophan is dependent of the localisation in the bone tissue. Osteocytes do present a higher tyrosine to tryptophan ratio than the matrix. Moreover, from our knowledge and personal experience, no other tissue does present a similar high level of tyrosine fluorescence.

Discussion

Several autofluorescent biomolecules can be observed inside isolated cells or in a tissue. During physiological and/or pathological processes the changes occurring in the cell and tissue result in modifications of the amount and distribution of those endogenous fluorophores and chemical-physical properties of their microenvironment. Therefore, monitoring the endogenous fluorophores distribution and the intensity of their fluorescence emission can give diagnosis insights and can help to understand biochemical transformations. While the spectral characteristics of isolated molecules can differ from physiological conditions, it is possible to identify them inside our chosen examples.

As for plant tissues, during plant-pathogen infection, the physiological state of the invaded tissues is altered. This can be reflected in changes in photosynthesis, transpiration or both. Fluorescence imaging is thus useful for visualization of emerging biotic stresses while detecting the chlorophyll fluorescence (endogenous fluorochrome, which mediates photosynthesis) or monitoring metabolic cell activity through detection of fluorescent coenzymes, such as NAD(P)H (Chaerle and Van der Straeten, 2001; Kasimova, 2006). In addition, the possibility to follow the spectroscopic state at micrometer scale of the major compounds without any markers is of importance for high yield recovery of vegetal wastes.

Nicotinamide adenine dinucleotide (NAD(P)H) and flavin adenine dinucleotide (FAD) are metabolic cofactors that act as electron donors and acceptors in the electron transport chain of the mitochondria, thus having a major role in metabolism pathways of eukaryotic cells. While the reduced form, NAD(P)H, is fluorescent and has an excitation maximum in the region of 350 nm with emission at 450 nm (Figure 1), the

oxidized form NAD^+, does not produce fluorescence (Paul and Schneckenburger, 1996; Kirkpatrick et al., 2005; Wang and Youle, 2009). Conversely, in the case of flavins, the fluorescent form is the oxidized form (excitation maximum at 450 nm with emission at 535 nm) and the reduced form does not fluoresce. Figure 6 shows the possibility of spatial detection of tryptophan and tyrosine-related fluorescence. One can envisage following the changes of tyrosine and tryptophan signal to monitor the proteins synthesis, degradation or both. Thus, synchrotron DUV microspectroscopy opens boundaries, since understanding of the spatial tryptophan and tyrosine signal changes, in relation to metabolic changes, may have both diagnostic as well as prognostic potential when treatment is concerned.

As for bone tissue, synchrotron UV microspectroscopy may give quantitative information on the cortical bone content of some autofluorescent molecules both in bone cells and their surrounding extracellular matrix. Results have shown that strong chronic alcohol consumption induced a decrease of the ratio tyrosine/tryptophan both in cell and surrounding matrix. This new methodology warrants a cell characterization *in situ* that allows evaluating osteocyte metabolism and gives a better understanding of the key role of this cell in the bone remodelling regulation. This local measurement of tyrosine and tryptophan levels may give a better understanding of cellular metabolism according to different physio-pathological conditions such as osteoporosis.

Many probes that are usually excited in the visible may be also excited in the UV range. For example, fluorescent proteins (FPs) can be excited either directly through their chromophore or by exciting the tryptophan residues that transfer their energy to the chromophore (Visser et al., 2005). This could lead to higher resolution studies of FPs by lowering their excitation wavelength. Moreover, this opens the possibility to

study simultaneously several different FPs with one single excitation of their respective tryptophan.

Moreover, many drugs and toxins do present fluorescence when excited in the DUV; it is then possible to follow their pharmacokinetic at tissular, cellular or subcellular level by directly following their fluorescence distribution without adding external probes or radiolabels (Diaspro et al., 2005). As an example in the area of material science, phenol- or diphenol-molecules, like Bisphenol A (BPA), exhibit absorption and fluorescence in DUV region (Del Olmo et al., 1999). BPA is used as a polymerization inhibitor in PVC while epoxy resins containing BPA are used as coatings on the inside of almost all food and beverage cans. As such, BPA leaching can occur when they are being treated with high temperature or extreme pH (Brede et al., 2003; Munguía-López et al., 2005). Because of health risk, one can envisage to use synchrotron DUV microspectroscopy to detect its presence at very low concentrations in food constituents and/or to use this technique to develop and validate sample preparations methods, which would lead to heath safe requirements.

Of note, the ideal drug to be followed in UV shall have an emission shifted from the tryptophan fluorescence (since tryptophan has strong contribution to autofluorescence signal), or to bypass the tryptophan fluorescence by an excitation outside the 240 to 300 nm range, or if not, then a drug with high quantum yield of fluorescence is required (order of higher than the autofluorescence signal). Otherwise, multivariate data treatment is required to separate the molecule of interest from the proteins fluorescence (Batard et al., 2001).

From the examples discussed above, we clearly showed that DUV microspectroscopy could monitor the numerous endogenous fluorophores and their

distribution on the tissular as well as cellular level. Note, working in monochromatic excitation mode, the light power is very low (μW). This allowed us to record the spectral map of living cells without detecting any changes in cell morphology during or after the measurement. As discussed above, measuring of live cell opens up possibility to follow the dynamic changes within the specimen. However, in experiments were dynamic processes are not issue; one can work with fixed specimens. Indeed, fixation with formaldehyde did not reveal any changes in autofluorescence of single cell when excited with 275 nm; e.g. for fixed as for live cells tryptophan fluoresced at 335 nm and tyrosine at 306 nm (data not shown). Although, the autofluorescence of cells and tissues is often (almost ever) considered as a parasitic signal that must be minimized; here, we demonstrate, that using the right experimental conditions, this so-called background signal, is rich in information and can become useful.

Material and Methods

Isolated auto fluorescent compounds

Chemicals: Pyridoxin, N-acetyl-L-tryptophanamide, N-acetyl-L-tyrosinamide, •-Nicotinamide adenine dinucleotide, reduced dipotassium salt (NADH), Alcohol dehydrogenase from Saccharomyces cerevisiae (ADH), Collagen type I, Elastin, phosphate-buffered saline (PBS), sodium hydroxide (NaOH) and TRIS were purchased from Sigma-Aldrich (Lyon, France). Acetic acid was purchased from Merck (Fontenay sous-Bois, France) and hydrogen chloride (HCl) from Carl Roth GmbH (Germany).

Preparation of solutions: Stock solution of Pyridoxine (c = 8.75×10^{-3}M) was prepared by dissolving pyridoxine powder in 1 M HCl. For recording the pyridoxine absorption and fluorescence spectra, the stock solution was diluted with PBS pH = 7.4 to a final concentration of 5×10^{-6}M. Collagen type I was first dissolved in 0.1 M acetic acid to a concentration of 1 mg/ml. The stock of collagen was then diluted with PBS pH = 7.4 to a final concentration of 0.074 mg/ml. Stock solution of Elastin (c = 1 mg/ml) was prepared by dissolving elastin powder in 1M NaOH, followed by dilution in PBS pH = 7.4 to a final concentration of 0.027 mg/ml. The N-acetyl-L-tryptophanamide and N-acetyl-L-tyrosinamide were both dissolved in 25×10^{-3}M Tris-HCl pH = 7.8 to obtain stock solutions concentrations of 8.15×10^{-3}M for N-acetyl-L-tryptophanamide and 6.39×10^{-3}M for N-acetyl-L-tyrosinamide respectively. Both stock solutions were then diluted to a concentration of 10×10^{-6} M for N-acetyl-L-tryptophanamide and 21.3×10^{-6} M for N-acetyl-L-tyrosinamide. Absorption and fluorescence spectra were measured immediately after dilution.

Preparation of NADH: ADH complexes: Stock solutions of NADH (c = $1.85x10^{-2}$ M) and stock solution of ADH (c = $2.83x10^{-3}$M) were prepared in 0.1M Tris-HCl pH = 8. Solutions of complexes were obtained by dilution of stock solutions of NADH and ADH with 0.1M Tris-HCl pH = 8. Three different complexes of NADH:ADH have been prepared at the following concentrations for both components: NADH ($10x10^{-6}$ M) : ADH ($1x10^{-4}$ M); NADH ($8.2x10^{-6}$ M) : ADH ($5x10^{-4}$ M) and NADH ($6.5x10^{-6}$ M) : ADH ($1x10^{-3}$ M). The absorption and fluorescence spectra of thus prepared solutions were measured immediately after mixing. In order to distinguish between the spectral characteristics of these components, the NADH and ADH were measured also individually: NADH in 0.1M Tris-HCl pH = 8 at $10x10^{-6}$ M concentration and ADH at $1.62x10^{-4}$ M concentration.

Absorption: To avoid inner filter effect in our fluorescence emission experiment, for each sample absorption spectrum was also measured. Absorption spectra were recorded at 20° C using UV-VIS spectrophotometer (Specord 210, Analytic Jena AG, Jena, Germany) in the 190-900 nm range with slits width corresponding to a resolution of 2 nm. For measurements, we used a 1 cm path length quartz cell.

Fluorescence: Fluorescence spectra were measured on optically diluted samples (i.e. absorption < 0.1 at the excitation wavelength) recorded at 20° C using a FluoroMax-4 (HORIBA Jobin Yvon INC, Chilly Mazarin, France) spectrofluorimeter. To record the excitation and emission spectra of individual compounds, the best excitation and emission wavelengths were chosen after optimisation (see Figure 2).

Para-coumaric acid, ferulic acid and lignin

Para-coumaric acid and ferulic acid were purchased from Sigma-Aldrich (Lyon, France). Powder was first dissolved in water at a concentration of 3.2 mg/mL and 2.6

mg/mL respectively. Samples were further diluted in water in order to obtain an absorbance value of about 0.03 when measured in 1 cm path length cuvettes. Fluorescence excitation and emission spectra were recorded on a Fluorolog-3 spectrophotometer (HORIBA Jobin Yvon INC, Chilly Mazarin, France), using 3 mm path length cuvettes (Hellma France, Paris). Lignin was observed as a powder in a special holder (HORIBA Jobin Yvon INC, Chilly Mazarin, France) in a front-face configuration. A long pass filter with a cut-off at 351 nm was inserted between sample and detector for ferulic acid measurement.

DUV microspectrometer

Microspectrofluorescence spectra were recorded on Polypheme, the DUV inverted microspectrofluorimeter installed at DISCO Beamline (Jamme et al., 2010). Excitation was provided by the continuous emittance from the DISCO beamline bending magnet at Synchrotron SOLEIL (Giuliani et al., 2009). While the system was already described elsewhere (Jamme et al., 2010), it is constructed around an Olympus IX71 inverted microscope stand with homemade replacement of the intermediate lenses that were not transparent in UV. Light detection is collected through a DUV lens and an adjustable pinhole. In order to suppress the Rayleigh band whatever the excitation wavelength, the detection system (T6400, Jobin-Yvon, Fr) uses a triple monochromator in a substractive mode. Thereafter, the fluorescence emission spectrum of the studied voxel is projected onto a -70°C peltier cooled iDus CCD (Andor) of 1024x256 pixels with a 26x26 µm pixel size and a 26.6x6.7 mm detector size and a dark current of less than 0.002e/pixel/sec. Spectra are recorded at a 1024 pixels depth and a 16 bits dynamic range.

Isolated cells

Cell line and culture condition: HeLa cells, a human cervix epithelial cell line, were a generous gift from Dr. Denis Biard from CEA-DSV-iRCM/INSERM U935, Institut A. Lwoff-CNRS, Villejuif Cedex, France. Cells were routinely cultured as monolayer and were grown in Dulbecco's modified Eagle's medium (DMEM) containing L-glutamine (862 mg L^{-1}), sodium pyruvate (110 mg L^{-1}) and glucose (4500 mg L^{-1}), supplemented with 10% fetal calf serum (FCS), penicillin (50 µg mL^{-1}) and streptomycin (50 µg mL^{-1}). All chemicals were obtained from Gibco Invitrogen (Villebon sur Yvette, France). The cells were maintained at 37°C in a humidified atmosphere of 5% CO_2. For the microscopic detection of endogenous fluorophores from HeLa cells, the cells were plated in plastic Petri dishes (35x10 mm) containing 25 mm round quartz coverslip (Cening, Cn) and incubated for 2 days. Cell attachment and growth was monitored by visible inspection using a microscope. Coverslip with desired cell growth confluence was rinsed in DMEM in absence of FCS or antibiotics for 1-2 minutes. Thereafter, the living cells were directly mounted on the microscope and spectra of cells in PBS were taken.

Maize stem cell walls

Maize from a reference genotype F2 were grown at INRA Lusignan and stems were harvested at the female flowering stage. The internodes under the ear were collected and stored in 70% (v/v) ethanol/water.

Samples were taken from the middle of maize internodes, embedded into paraffin and sectioned using a microtome (Jamme et al., 2008). Proteins were removed using a protease enzyme named subtilisin A type VIII, bacterial, from bacillus licheniformis. Preliminary results showed that 10 µm thick sections were adapted for fluorescence

spectral acquisitions. Sections were collected on ZnS windows. A region corresponding to a vascular bundle near the epidermis was selected as showing a chemical variability according to cell types (Figure 7) (Jung and Casler, 2006).

Bones

These studies were approved by the National Institute for Health and Medical Research (INSERM). The procedure for the care and killing of the animals was in accordance with the European Community standards on the care and use of laboratory animals (Ministère de l'agriculture, France, Authorisation INSERM45-001). Wistar male rats (8 weeks old at baseline) were chosen at random and assigned to one of the three following groups: controls and two different percentages ethanol beverage (25% v/v and 35% v/v) during 19 weeks. After the sacrifice, tibias were dissected free of connective and fat tissue. They were fixed in a 4% v/v formalin solution and kept at + 4°C. As required the tibias were cut transversally in slices (thickness 300 µm) in the superior third part of the diaphysis, with a high speed rotary tool (Dremel 300, Dremel, USA).

UV monochromatised light (typically between 270 and 330 nm) was used to excite cortical bone sections through a 40× ultrafluar objective (Zeiss, Germany). The fluorescence emission spectrum arising from each excited pixel is recorded. Rastering of the sample allows one to record x, y, lambda, I maps of interest [2]. Mapping of 20 × 20 μm^2 was performed with a 2•2 µm step size, chosen by considering the relative size of the cells and the area to be scanned, with a 5 s acquisition time per spectrum. The Region of Interest (ROI) was centred on the osteocyte. For each rat sample, 3 acquisitions were achieved both in osteocytes ROI and surrounding matrix ROI.

Author contributions

F.J., S.V. and M.R. conceived and designed the research; F.J., S.K., S.V., F.A. and V.R. carried out the experiments; F.A. and S.P. provided some of the samples; F.J., S.K, S.V. and M.R analysed the data; F.J., S.K., S.V. and M.R. wrote the article.

References

Allouche, F., Hanafi, M., Jamme, F., Robert, P., Guillon, F., Devaux, M.F. (2012) Coupling hyperspectral image data having different spatial resolutions by extending multivariate inter-battery Tucker analysis. Chemometr. Intell. Lab. **113(1)**, 43-51

Anderson, W., Akin, D. (2008) Structural and chemical properties of grass lignocelluloses related to conversion for biofuels. J. Ind. Microbiol. Biot. **35**, 355–366

Batard, E., Jamme, F., Villette, S., Jacqueline, C., de la Cochetière, M. F., Caillon, J., Réfregiers, M. (2011) Diffusion of ofloxacin in the endocarditis vegetation assessed with synchrotron radiation UV fluorescence microspectrocopy. PLoS ONE **6**

Brede, C., Fjeldal, P., Skjevrak, I., Herikstad, H. (2003) Increased migration levels of bisphenol A from polycarbonate baby bottles after dishwashing, boiling and brushing. Food Addit. Contam. **20**, 684–689

Chaerle, L., Van der Straeten, D. (2001) Seeing is believing: imaging techniques to monitor plant health. B.B.A. Gene Struct. Expr. **1519**, 153-166

Cox, S., Rosten, E., Monypenny, J., Jovanovic-Talisman, T., Burnette, D.T., Lippincott-Schwartz, J., Jones, G.E., Heintzmann, R. (2011) Bayesian localization microscopy reveals nanoscale podosome dynamics. Nat Meth **9**, 195–2001.

Del Olmo, M., Zafra, A., Navas, N. (1999) Trace determination of phenol, bisphenol A and bisphenol A diglycidyl ether in mixtures by excitation fluorescence following micro liquid–liquid extraction using partial least squares regression. Analyst **124**, 385-390

Diaspro, A., Chirico, G., Collini, M. (2005) Two-photon fluorescence excitation and related techniques in biological microscopy, Q. Rev. Biophys **38(2)**, 97-166

Giuliani, A., Jamme, F., Rouam, V., Wien, F., Giorgetta, J. L., Lagarde, B., Chubar, O., Bac, S., Yao, I., Rey, S., Herbeaux , C., Marlats, J. L., Zerbib, D., Polack, F., Réfregiers, M. (2009) DISCO: a low-energy multipurpose beamline at synchrotron SOLEIL. J. Sync. Rad. **16** 835–841

Jamme, F., Robert, P., Bouchet, B., Saulnier, L., Dumas, P., Guillon, F. (2008) Aleurone cell walls of wheat grain: high spatial resolution investigation using synchrotron infrared microspectroscopy. Appl. Spectrosc. **62**, 895–900

Jamme, F., Villette, S., Giuliani, A., Rouam, V., Wien, F., Lagarde, B., Réfrégiers, M. (2010) Synchrotron UV fluorescence microscopy uncovers new probes in cells and tissues. Microsc. Microanal. **16**, 507–514

Jung, H.G., Casler, M.D. (2006) Maize Stem Tissues. Crop Science **46**, 1793-1800

Kanick, S., Van der Leest, C., Aerts, J. (2010) Integration of single-fiber reflectance spectroscopy into ultrasound-guided endoscopic lung cancer staging of mediastinal lymph nodes. J. Biomed. Opt. **15**, 017004

Kasimova, M.R. (2006) The free NADH concentration is kept constant in plant mitochondria under different metabolic conditions. Plant Cell **18**, 688–698

Kirkpatrick, N., Zou, C., Brewer, M. (2005) Endogenous Fluorescence Spectroscopy of Cell Suspensions for Chemopreventive Drug Monitoring. Photochem. Photobiol. **81**, 125-134

Kohler, A. (1904) A microphotographic device for ultraviolet light (lambda=275 mu) and investigations into organic tissues using this device. Phys. Z. **5**, 666–673

Lakowicz, J.R. (2006) Principles of Fluorescence Spectroscopy. Boston: Springer US

Ludford, R.J., Smiles, J., Welch, F.V. (1948) Ultra-Violet microscopy of living malignant cells. Nature **162**, 650–651

Mellors, R.C., Berger, R.E., Streim, H.G. (1950) Ultraviolet Microscopy and Microspectroscopy of Resting and Dividing Cells: Studies with a Reflecting Microscope. Science **111**, 627–632

Munguía-López, E.M., Gerardo-Lugo, S., Peralta, E., Bolumen, S., Soto-Valdez, H. (2005) Migration of bisphenol A (BPA) from can coatings into a fatty-food simulant and tuna fish. Food Addit. Contam. **22**, 892–898

Paul, R.J., Schneckenburger, H. (1996) Oxygen concentration and the oxidation-

reduction state of yeast: determination of free/bound NADH and flavins by time-resolved spectroscopy. Naturwissenschaften **83**, 32–35

Pavlova, I., Williams, M., El-Naggar, A., Richards-Kortum, R., Gillenwater, A. (2008) Understanding the biological basis of autofluorescence imaging for oral Cancer detection: high-resolution fluorescence microscopy in viable tissue. Clin. Cancer Res. **14**, 2396–2404

Petit, V.W., Réfregiers, M., Guettier, C., Jamme, F., Sebanayakam, K., Brunelle, A., Laprévote, O., Dumas, P., Le Naour, F. (2010) Multimodal spectroscopy combining time-of-flight-secondary ion mass spectrometry, synchrotron-FT-IR, and synchrotron-UV microspectroscopies on the same tissue section. Anal. Chem. **82**, 3963–3968

Ramanujam, N. (2000) Fluorescence spectroscopy of neoplastic and non-neoplastic tissues. Neoplasia (New York)

Ramanujam, N., Mitchell, M.F., Mahadevan, A., Warren, S., Thomsen, S., Silva, E., Richards-Kortum, R. (1994) In vivo diagnosis of cervical intraepithelial neoplasia using 337-nm-excited laser-induced fluorescence. Proc. Natl. Acad. Sci. USA **91**, 10193–10197

Robert, P., Jamme, F., Barron, C., Bouchet, B., Saulnier, L., Dumas, P., Guillon, F. (2010) Change in wall composition of transfer and aleurone cells during wheat grain development. Planta **223**, 393-406

Rochefort, G.Y., Pallu, S., Benhamou, C.L. (2010) Osteocyte: the unrecognized side of bone tissue. Osteoporos. Int. **21**, 1457–1469

Saadi, A., Lempereur, I., Sharonov, S., Autran, J. C., Manfait, M. (1998) Spatial

Distribution of Phenolic Materials in Durum Wheat Grain as Probed by Confocal Fluorescence Spectral Imaging. J. Cereal Sci. **28**, 107–114

Tawil, G., Jamme, F., Réfregiers, M., Viksø-Nielsen, A., Colonna, P., Buléon, A. (2011) In situ tracking of enzymatic breakdown of starch granules by synchrotron UV fluorescence microscopy. Anal. Chem. **83**, 989–993

Villette, S., Pigaglio-Deshayes, S., Vever-Bizet, C., Validire, P., Bourg-Heckly, G.V. (2006) Ultraviolet-induced autofluorescence characterization of normal and tumoral esophageal epithelium cells with quantitation of NAD(P)H. Photochem. Photobiol. Sci. **5**,483-492

Visser, N.V., Borst, J.W., Hink, M.A., van Hoek, A., Visser, A.J.W.G. (2005) Direct observation of resonance tryptophan-to-chromophore energy transfer in visible fluorescent proteins. Biophys. Chem. **116**, 207–212

Wagnieres, G., Star, W., Wilson, B. (1998) In vivo fluorescence spectroscopy and imaging for oncological applications. Photochem. Photobiol. **68**, 603–632

Wang, C., Youle, R.J. (2009) The role of mitochondria in apoptosis. Annu. rev. genet. **43**, 95-118

Zeskind, B.J., Jordan, C.D., Timp, W., Trapani, L., Waller, G., Horodincu, V., Ehrlich, D.J., Matsudaira, P. (2007) Nucleic acid and protein mass mapping by live-cell deep-ultraviolet microscopy. Nat. Meth. **4**, 567–569

Zipfel, W.R., Williams, R.M., Christie, R., Nikitin, A.Y., Hyman, B.T., Webb, W.W. (2003) Live tissue intrinsic emission microscopy using multiphoton-excited native fluorescence and second harmonic generation. Proc. Natl. Acad. Sci. USA **100**, 7075–7080

Legend

Figure 1: Fluorescence excitation spectra of the main autofluorescent contributors found in mammalian cells and tissues. Maxima of excitation are presented following the name of the compound. Within brackets is indicated the emission wavelength at which was recorded the excitation spectrum.

Figure 2: Fluorescence emission spectra of the main autofluorescent contributors observable in mammalian cells and tissues. Maxima of emission are presented following the name of the compound. Within brackets is indicated the excitation wavelength at which was recorded the emission spectrum.

Figure 3: Fluorescence excitation spectra of the main autofluorescent contributors found in plant tissues: lignin, para-coumaric and ferulic acids.

Figure 4: Fluorescence emission spectra of the main autofluorescent contributors found in plant tissues: lignin, para-coumaric and ferulic acids.

Figure 5: (a) Spectral distribution of the photon flux delivered to the sample and (b) relative response of the microscope over the whole spectral range.

Figure 6: (a) Transmission image of a living single Hela cell, (b) corresponding sum intensity spectral image and (c) spectrum of the grey pixel. The gaussian deconvolution presents two main components: tryrosine and tryptophan. Pixel size 1.5 x 1.5 μm^2

Figure 7: (a) Transmission image of a maize stem section, (b) corresponding sum intensity spectral image and (c) average spectra of the three cell types. Scale bar 4 microns.

Figure 8: (a) Mouse bone tissue transmission image showing the localization of the osteocyte inside the bone matrix and (b) typical spectra of matrix and osteocyte recorded from 1x1 μm^2 pixels (bottom). Scale bar 8 microns.

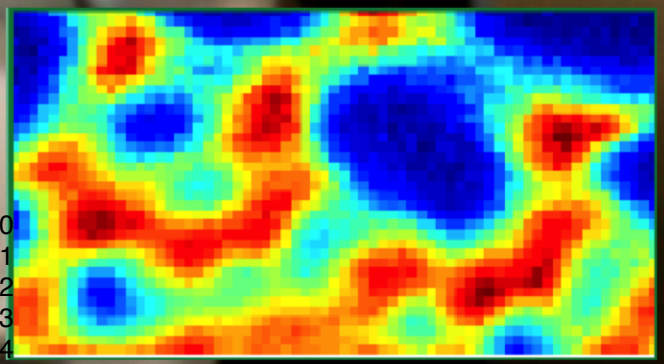

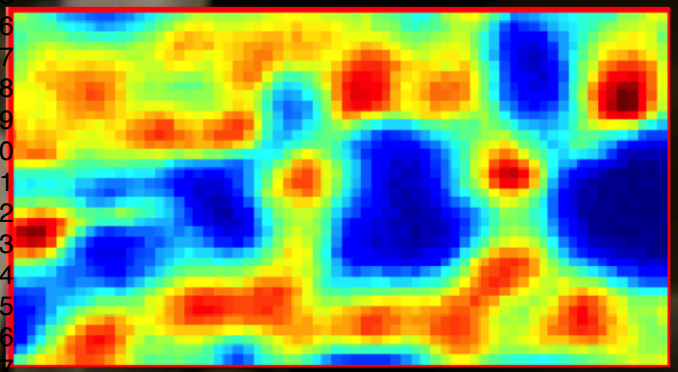

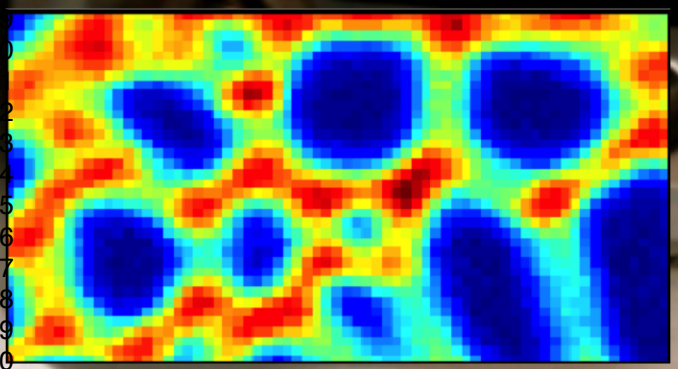

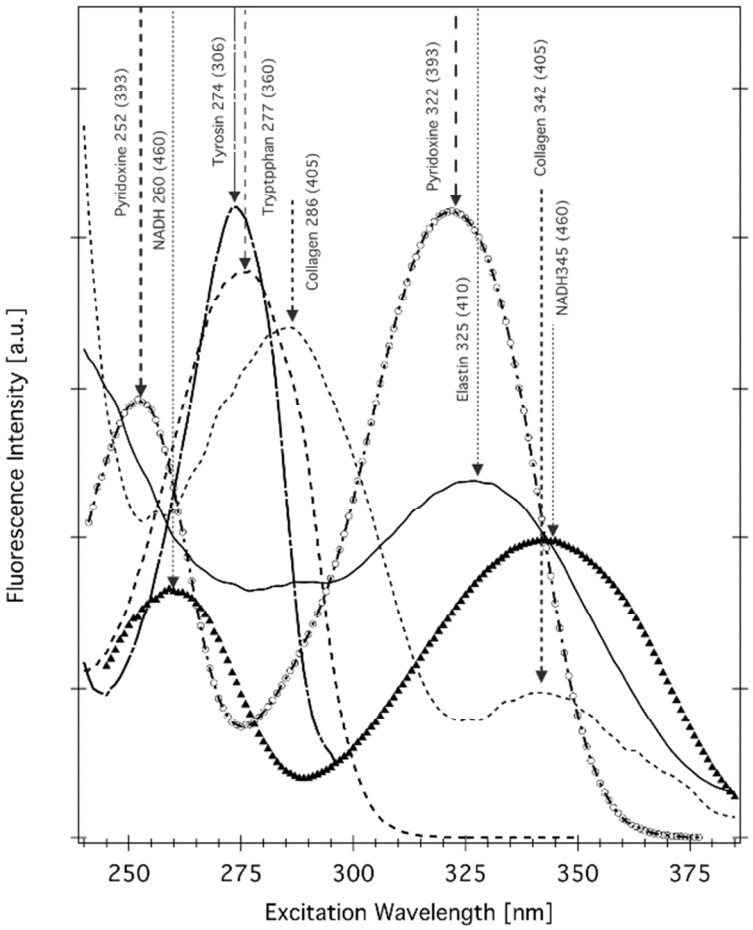

Figure 1: Fluorescence excitation spectra of the main autofluorescent contributors found in mammalian cells and tissues. Maxima of excitation are presented following the name of the compound. Within brackets is indicated the emission wavelength at which was recorded the excitation spectrum.
296x278mm (72 x 72 DPI)

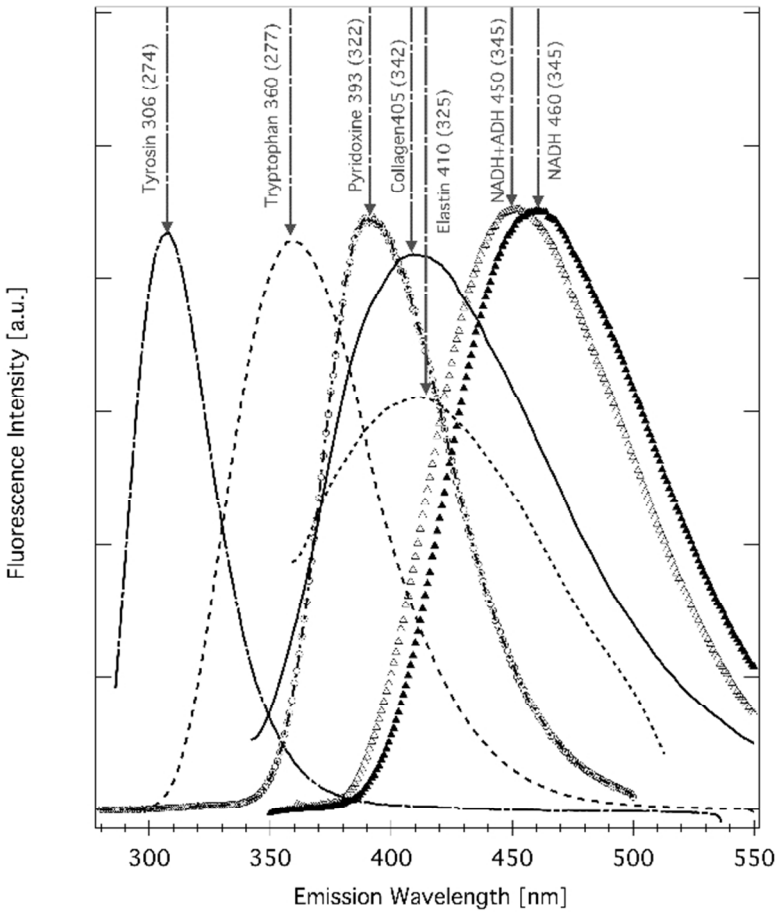

Figure 2: Fluorescence emission spectra of the main autofluorescent contributors observable in mammalian cells and tissues. Maxima of emission are presented following the name of the compound. Within brackets is indicated the excitation wavelength at which was recorded the emission spectrum.
298x275mm (72 x 72 DPI)

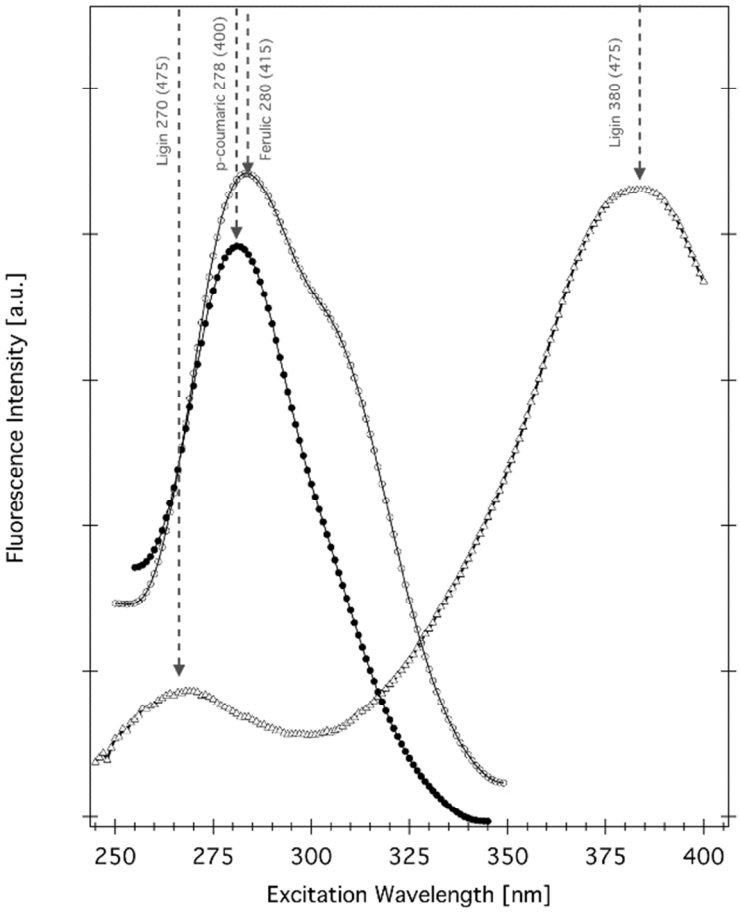

Figure 3: Fluorescence excitation spectra of the main autofluorescent contributors found in plant tissues: lignin, para-coumaric and ferulic acids.
300x277mm (72 x 72 DPI)

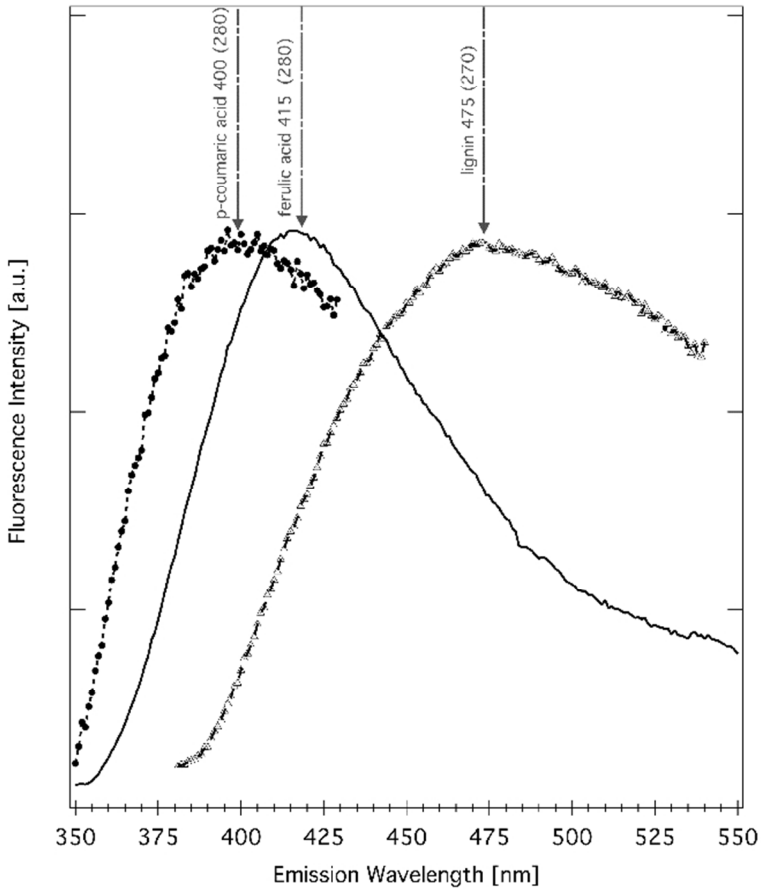

Figure 4: Fluorescence emission spectra of the main autofluorescent contributors found in plant tissues: lignin, para-coumaric and ferulic acids.
306x275mm (72 x 72 DPI)

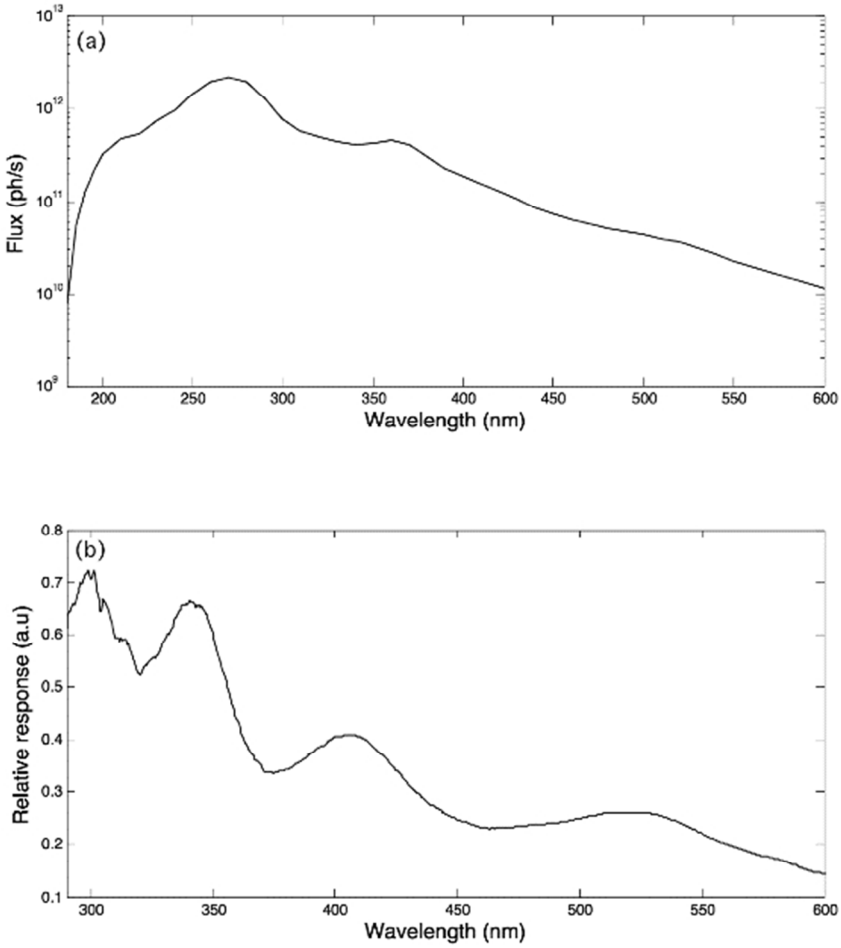

Figure 5: (a) Spectral distribution of the photon flux delivered to the sample and (b) relative response of the microscope over the whole spectral range.
215x279mm (72 x 72 DPI)

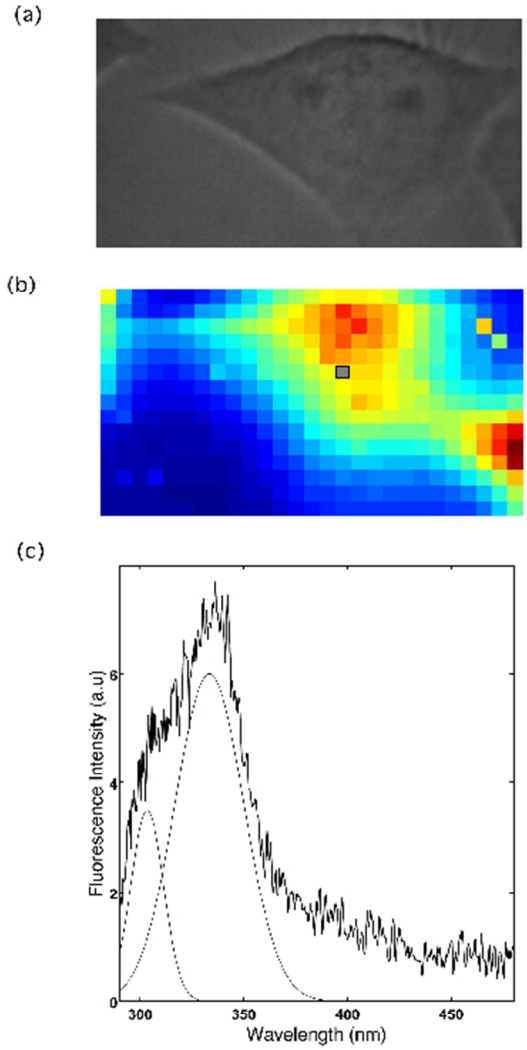

Figure 6: (a) Transmission image of a living single Hela cell, (b) corresponding sum intensity spectral image and (c) spectrum of the grey pixel. The gaussian deconvolution presents two main components: tryrosine and tryptophan. Pixel size 1.5 x 1.5 µm2
209x297mm (72 x 72 DPI)

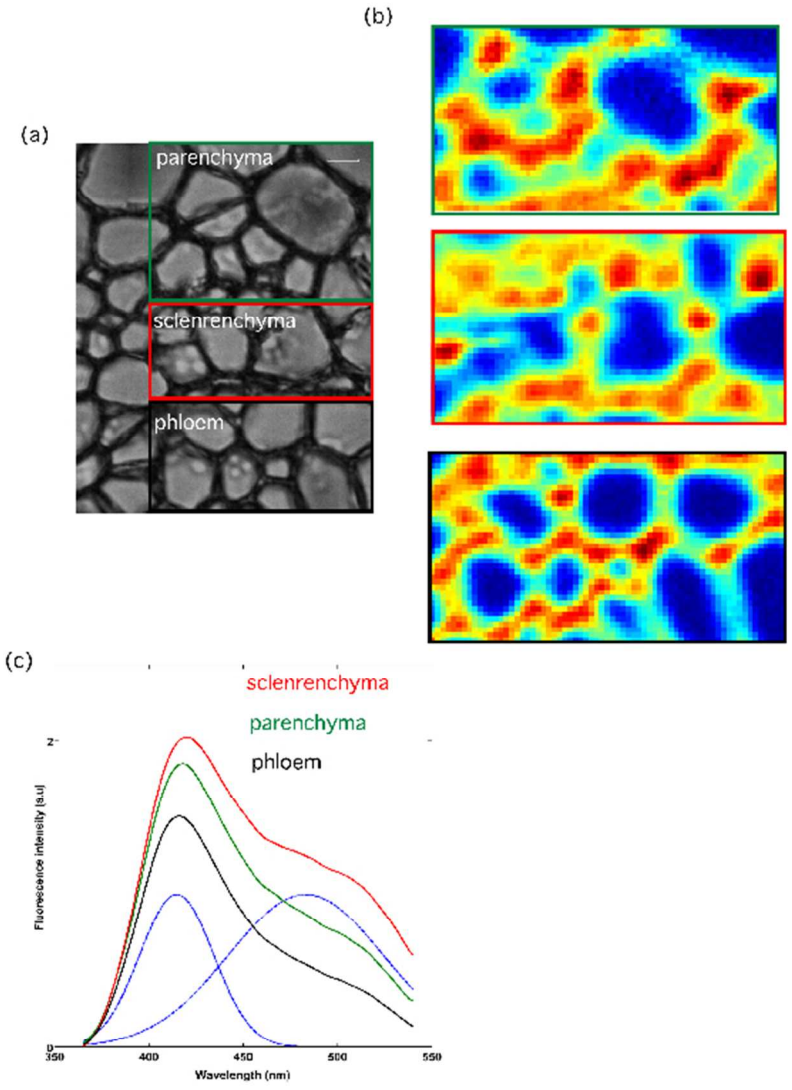

Figure 7: (a) Transmission image of a maize stem section, (b) corresponding sum intensity spectral image and (c) average spectra of the three cell types. Scale bar 4 microns.
209x297mm (72 x 72 DPI)

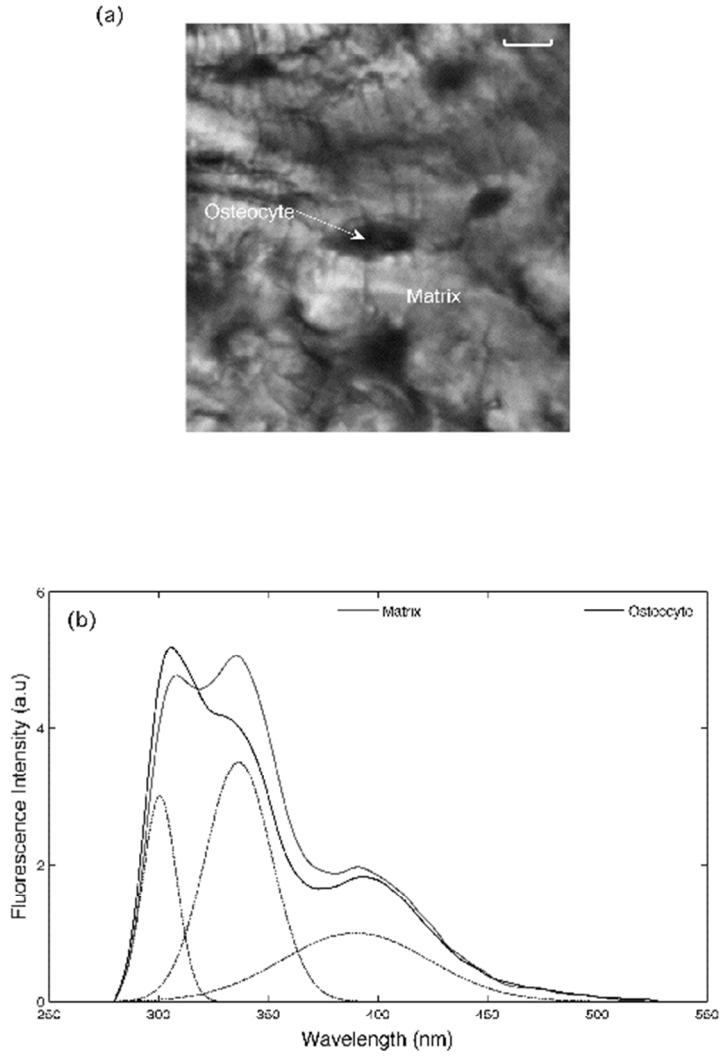

Figure 8: (a) Mouse bone tissue transmission image showing the localization of the osteocyte inside the bone matrix and (b) typical spectra of matrix and osteocyte recorded from 1x1 µm2 pixels (bottom). Scale bar 8 microns.
210x297mm (72 x 72 DPI)